

Simple Floquet-Wannier-Stark-Andreev viewpoint and emergence of low-energy scales in a voltage-biased three-terminal Josephson junction

Régis Mélin

*Centre National de la Recherche Scientifique, Institut NEEL, F-38042 Grenoble Cedex 9, France and
Université Grenoble-Alpes, Institut NEEL, F-38042 Grenoble Cedex 9, France*

Jean-Guy Caputo

Laboratoire de Mathématiques, INSA de Rouen, Avenue de l'Université, F-76801 Saint-Etienne du Rowray, France

Kang Yang

*Laboratoire de Physique Théorique et des Hautes Energies,
CNRS UMR 7589, Université Pierre et Marie Curie,
Sorbonne Universités, 4 Place Jussieu, 75252 Paris Cedex 05 and
Laboratoire de Physique des Solides, CNRS UMR 8502,
Univ. Paris-Sud, Université Paris-Saclay F-91405 Orsay Cedex, France*

Benoît Douçot

*Laboratoire de Physique Théorique et des Hautes Energies,
CNRS UMR 7589, Université Pierre et Marie Curie,
Sorbonne Universités, 4 Place Jussieu, 75252 Paris Cedex 05*

A three-terminal Josephson junction consists of three superconductors coupled coherently to a small nonsuperconducting island, such as a diffusive metal, a single or double quantum dot. A specific resonant single quantum dot three-terminal Josephson junction (S_a, S_b, S_c) biased with voltages $(V, -V, 0)$ is considered, but the conclusions hold more generally for resonant semi-conducting quantum wire set-ups. A simple physical picture of the steady state is developed, using Floquet theory. It is shown that the equilibrium Andreev bound states (for $V = 0$) evolve into nonequilibrium Floquet-Wannier-Stark-Andreev (FWS-Andreev) ladders of resonances (for $V \neq 0$). These resonances acquire a finite width due to multiple Andreev reflection (MAR) processes. We also consider the effect of an extrinsic line-width broadening on the quantum dot, introduced through a Dynes phenomenological parameter. The DC-quartet current manifests a cross-over between the extrinsic relaxation dominated regime at low voltage to an intrinsic relaxation due to MAR processes at higher voltage. Finally, we study the coupling between the two FWS-Andreev ladders due to Landau-Zener-Stückelberg transitions, and its effect on the cross-over in the relaxation mechanism. Three important low-energy scales are identified, and a perspective is to relate those low-energy scales to a recent noise cross-correlation experiment [Y. Cohen *et al.*, arXiv:1606.08436].

I. INTRODUCTION

A BCS superconductor is characterized by a macroscopic classical ground state (the condensate) separated by a finite energy gap Δ from the first excited states (the superconducting quasiparticles). Superconducting materials such as those used in quantum nano-electronics support a tiny density of midgap states because of electron-electron or electron-phonon processes. The first investigations of quasiparticle relaxation times were carried out in the seventies^{1,2}. Inelastic electron-electron or electron-phonon interactions in the superconductors produce relaxation times τ_{e-e} and τ_{e-ph} respectively, thus with corresponding characteristic energies \hbar/τ_{e-e} and \hbar/τ_{e-ph} . Those energies for relaxation are accounted for phenomenologically by the so-called Dynes parameter, in the form of small imaginary part η_S added to the otherwise real-valued energy of superconducting quasiparticles. The Dynes parameter corresponds to a single parameter η_S for relaxation, accounting phenomenologically for both electron-electron and electron-phonon pro-

cesses. If τ_{e-e} and τ_{e-ph} have different orders of magnitude, then η_S can be approximated by the dominant mechanism, corresponding to taking the maximum between \hbar/τ_{e-e} and \hbar/τ_{e-ph} . Once processed with a small imaginary part η_S in energy, BCS theory produces the expected finite life-time \hbar/η_S for quasiparticles. The gap singularity threshold is also rounded, and, as mentioned above, a nonvanishingly small density of states is induced inside the superconducting gap.

A few experimentally relevant situations reveal spectacularly the importance of taking relaxation into account. Let us mention the noise of a two-terminal superconducting point contact at equilibrium³⁻⁵ where the direction of the current flow is reversed at random by thermal fluctuations, producing telegraph noise in the Cooper pair current. The noise is inverse proportional to the Dynes parameter in some window of parameters (the smaller electron-electron or electron-phonon inelastic scattering, the larger the signal.) The following paper brings physical answers in a situation resembling that of Refs. 3 and 4, in which electron-electron or electron-

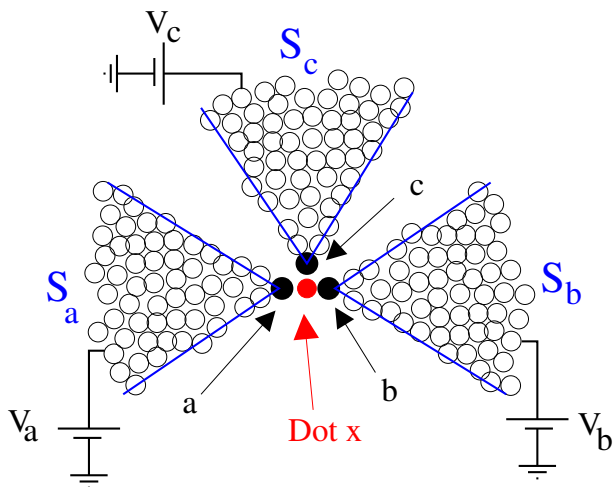


FIG. 1: *The three-terminal set-up*: The figure shows a zero-dimensional quantum dot connected to three superconductors. The three tunnel couplings between the dot x and S_a , S_b and S_c take identical values. The voltages are such that $V_a = -V_b \equiv V$ (with $V_c = 0$ the reference voltage), and the phases are denoted by $(\varphi_a, \varphi_b, \varphi_c)$. The quartet phase $\varphi_Q = \varphi_a + \varphi_b - 2\varphi_c$ is the relevant static phase combination for DC-transport and noise. The quantum dot x is shown as a zero-dimensional object because this is the limit in which the calculations are carried out. The corresponding Hamiltonian is given in Appendix.

phonon inelastic scattering cannot be discarded. One of the goals of the present work is to pave the way to a future theoretical investigation of the recent noise cross-correlation experiment of the Weizmann group⁶ (see the concluding Sec. IV B). In view of Refs. 3,4, this requires handling finite values for the Dynes parameters as it is done here. High sensitivity measurements⁷ of Dynes parameter smaller than $\sim 10^{-7}\Delta$ in Aluminum were reported recently, in connection with the realization of an electron turnstile^{8–10}. Quasiparticle poisoning^{11–14} is not captured explicitly by the present-time version of our model, which is nevertheless predictive as far as relaxation due multiple Andreev reflections (MARs) coupling the quantum dot to the semi-infinite quasiparticle continua is concerned.

Now that the sources of relaxation have been introduced, it is a matter of fact that an additional terminal does not produce only small changes in physics: Novel phenomena take place with three terminals, which were not there with two terminals. Let us mention the appearance of a static phase variable for specific voltage configurations¹⁵, leading to emergence of a Josephson-like current. Correlations among Cooper pairs is the mechanism for this DC-superflow in a voltage-biased three-terminal Josephson junction. Fig. 1 shows such a set-up, in which three superconducting electrodes are connected to a single quantum dot. (Going from three to four terminals is a non trivial step which produces also unexpected effects: for instance, emergence of topological

effects in a four-terminal Josephson junction¹⁶.) Three-terminal Josephson junctions have been the subject of experimental investigations in two different groups: with metallic structures¹⁷, and with semi-conducting quantum wires⁶. Besides metallic structures^{18–20}, experimental set-ups in the close-by field of Cooper pair splitting are realized with double quantum dots formed in carbon nanotubes²¹ or with semi-conducting quantum wires^{22,23}.

As mentioned above, the noise cross-correlations of a voltage-biased three-terminal Josephson junction were measured recently by the Weizmann group⁶. Current cross-correlations were measured in this experiment, in addition to providing evidence for the predicted resonant thresholds related to the gap edge singularities^{24,25}. Experimental evidence was obtained for supercurrent of “quartets” if the condition $V_a + V_b = 0$ on bias voltages is fulfilled ($V_c = 0$ for the grounded S_c , and $V_a = -V_b \equiv V$ for S_a and S_b). The previous pioneer Grenoble experiment¹⁷ had already reported a similar anomaly for the DC-current response in a metallic structure, but without measurement of current cross-correlations as it was done in Ref. 6. A relevant modeling for the Weizmann group experiment⁶ is that of a resonant double quantum dot connected to three BCS superconductors S_a , S_b and S_c , and biased at voltages V_a , V_b and V_c .

The initial theoretical proposals for Cooper pair splitting^{26–32} were based on observation that pairs of entangled electrons can be extracted from a classical BCS condensate, and be split as two spin- and energy-entangled quasiparticles transmitted in two different normal or ferromagnetic leads. Forming virtual states with four (instead of two) entangled quasiparticles is surprisingly possible in a three-terminal Josephson junction. A quartet^{15,33–37} consists of four fermions emanating from two pairs in the grounded S_c , which interchange partners, recombine as two outgoing pairs in S_a and S_b , and eventually disappear in the condensates of S_a and S_b . The overall process is DC, and compatible with energy conservation because of the specific condition $V_a + V_b = 0$ on the voltage configuration. However, the supercurrent due to the quartet or multipair mechanism¹⁵ and the corresponding noise cross-correlations³⁸ are phase-sensitive, and individual quasiparticles made of four fermions can hardly be dissociated from the collective superflow in which those are embedded. The situation for the quartets has thus its own specificities in comparison with collective excitations such as quasiparticles in the quantum Hall effect, having fractional charge.

Voltage-biased three-terminal Josephson junctions are representative of a class of time-periodic quantum Hamiltonians, which is a matter of Floquet wave-functions. While realizing this work, numerical data accumulated, and a stage was reached at which physical pictures and interpretations emerged from those “numerical experiments”. In this respect, the FWS-Andreev viewpoint (Floquet theory combined with band theory in the context of superconducting set-ups) appears to be the

right starting point. More precisely, the FWS-Andreev resonances are organized within two alternating FWS-Andreev ladders arising from the two equilibrium Andreev bound states at positive and negative energies. Those FWS-Andreev resonances (being nonequilibrium Andreev resonances) form “ladders” because those are replicated to infinity by Floquet theory, due to the periodic time-dependence of the Hamiltonian. An expression for the energies of the FWS ladders of Andreev resonances isolated from the quasiparticle semi-infinite continua is obtained within a few lines of calculations from Bohr-Sommerfeld quantization (see Sec. II in the paper, and Sec. VI in Supplemental Material). The Floquet energies can be also evaluated with Green’s functions (see Sec. VII in Supplemental Material): after lengthy calculations, the fully nonperturbative Bohr-Sommerfeld quantization result is recovered only in a given limiting case. This provides evidence for the power of the FWS-Andreev viewpoint for making analytical calculations, as opposed to Green’s function based on resummed perturbation theory in the coupling between the dot and the superconducting leads. The FWS-Andreev viewpoint proceeds with a different perturbation theory in the strength of the exponentially weak processes coupling the quantum dot to the quasiparticle continua above the gaps, and in the strength of Landau-Zener-Stückelberg transitions³⁹. Similarities between an equilibrium DC-supercurrent (in a phase-biased two-terminal Josephson junction) and the nonequilibrium DC-current due to the quartet or multipair mechanism in a three-terminal Josephson junction are considered in the following. This discussion is based on the discovery reported below of several relevant low-energy scales in the current, and in the FWS spectrum of Andreev resonances.

The paper is organized as follows. The FWS-Andreev viewpoint is presented in Sec. II. Numerical calculations are presented in Sec. III. Summary and perspectives are provided in the concluding Sec. IV. The Hamiltonian is provided in Appendix.

More technical discussions are relegated to Supplemental Material: details on the demonstration of the adiabatic theorem (Secs. I and II in Supplemental Material), principle of the code with finite η_{dot}/Δ (Sec. III in Supplemental Material). The failure of the Keldysh dressing algorithm with fully discrete spectrum is demonstrated (Sec. IV in Supplemental Material). The principle of another code based on the Floquet-Lippmann-Schwinger dressing algorithm is given in Sec. V of Supplemental Material. Sec. VI in Supplemental Material presents a complementary and more general introduction to FWS ladders, not necessarily in the context of superconductivity. The Rabi frequencies are calculated in Sec. VII of Supplemental Material from the rotating wave approximation, and from microscopic Green’s functions. A detailed physical discussion of the nonstandard generalized Dynes parameter is presented in Sec. VIII of Supplemental Material.

II. FLOQUET-WANNIER-STARK-ANDREEV VIEWPOINT

A. Two-terminal junctions

Floquet theory can be introduced for a general time-periodic Hamiltonian^{40,41} (see also Sec. VI in Supplemental Material), but its physical meaning becomes rather transparent in the context of superconducting junctions. The Josephson relation implies a time-periodic Hamiltonian (see Appendix) for the Hamiltonian of the three-terminal set-up in Fig. 1). The gauge can be chosen in such a way as to get rid of the time dependence of the Hamiltonian, and to handle instead (now for a two-terminal junction):

$$\tilde{\mathcal{H}} = \hat{\mathcal{H}}_a + \hat{\mathcal{H}}_b + \hat{\mathcal{H}}_{a-b} - eV (\hat{N}_a - \hat{N}_b), \quad (1)$$

where $\hat{\mathcal{H}}_a$ and $\hat{\mathcal{H}}_b$ are the BCS Hamiltonians of the two superconducting leads S_a and S_b coupled by the tunnel term $\hat{\mathcal{H}}_{a-b}$. The term $-eV(\hat{N}_a - \hat{N}_b)$ is the energy of the $N_a - N_b$ fermions which have been transmitted between the two electrodes. Eq. (1) is supplemented with the commutation relation

$$\left[\hat{N}_a - \hat{N}_b, \frac{\hat{\varphi}_a - \hat{\varphi}_b}{2} \right] = i, \quad (2)$$

which makes this problem quantum mechanical. It is illustrative to plot $l = (N_a - N_b)/2$ on the x -axis and energy on the y -axis (see Fig. 2), not taking Eq. (2) into account in a first step. Two semi-classical energy bands are obtained for $l = 0$ (spanned by the two equilibrium Andreev bound states at positive and negative energies), and increasing $l = (N_a - N_b)/2$ produces the tilt shown in Fig. 2, due to the term $2eVl = eV(N_a - N_b)$ subtracted to the Hamiltonian. The semi-infinite quasiparticle continua are also shown in this tilted band picture.

Now, quantum mechanics is introduced. The Floquet wave-functions are evaluated and the corresponding resonant levels are quantized. The FWS-Andreev wave-functions are located essentially in the classically allowed regions (filled blue regions in Fig. 2b), and those are evanescent in the classically forbidden regions. Considering first two isolated FWS-Andreev bands, the expression of the resonant level energies is obtained from Bohr-Sommerfeld semi-classical quantization on the Floquet wave-function. Tunneling into quasi-particle continua will produce a finite line-width for the FWS-Andreev resonances.

Eigenstates of the extended Hamiltonian $\pm E(\hat{\varphi}) - 2eV\hat{l}$ are obtained, where $\hat{\varphi} = \hat{\varphi}_a - \hat{\varphi}_b$. In this expression, $E(\varphi)$ is the energy-phase relation of the upper bound state, and \pm refers to Andreev bound states at positive and negative energies respectively. The term $-2eV\hat{l}$ is the energy of the number $\hat{l} = (\hat{N}_a - \hat{N}_b)/2$ of pairs which have been transmitted during the quantum process. The trick is to note that \hat{l} and $\hat{\varphi}$ are canonically conjugate

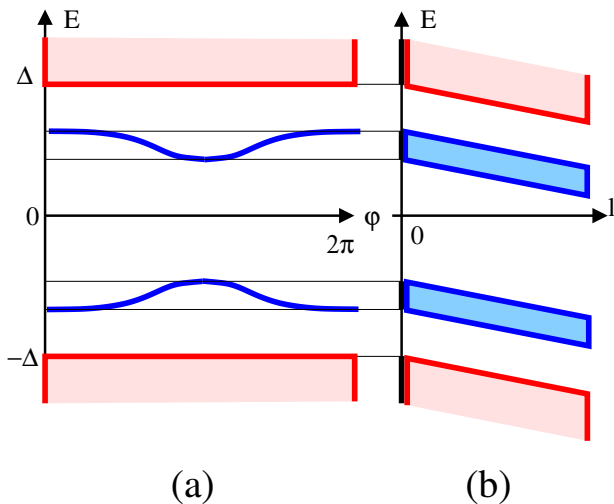


FIG. 2: *The FWS-Andreev tilted band picture*: Panel a shows the schematics for the energy-phase relation of a two-terminal Josephson junction with an embedded quantum dot supporting a single energy level, with two Andreev levels at opposite energies. Panel b shows how the tilted band picture in the (l, E) plane is related to the energy-phase relation, where $l = (N_a - N_b)/2$ (with N_a and N_b the number of fermions transmitted in S_a and S_b). The quasiparticle continua are shown in red. The dispersion of the two Andreev bound states is shown in blue on panel a. The filled blue region on panel b shows the FWS-Andreev bands. The noncolored regions are classically forbidden. It is supposed on this figure that the two superconducting leads are asymmetrically coupled to the quantum dot, therefore providing a gap between Andreev bound states for all values of the phase difference.

variables; see Eq. (2), which is equivalent to $[\hat{l}, \hat{\varphi}] = i$. The operator \hat{l} is then exactly identical to $\hat{l} = i\partial/\partial\varphi$. The Schrödinger equation in extended space takes the form of a first-order differential equation for the variable φ (see Sec. VI in Supplemental Material). The solution for the wave-function takes the form

$$\psi_{\pm}(\varphi) \sim \exp\left(\frac{i}{2eV} \int_0^{\varphi} (E \mp E(\varphi')) d\varphi'\right). \quad (3)$$

Imposing 2π -periodicity leads to the following quantized energies of the FWS-Andreev resonant levels:

$$E_j = 2eVj + \langle E \rangle \quad (4)$$

$$E_{j'} = 2eVj' - \langle E \rangle, \quad (5)$$

where j and j' are integers, and $\langle E \rangle$ denotes the average over the phase of the energy of the upper Andreev bound state:

$$\langle E \rangle = \frac{1}{2\pi} \int_0^{2\pi} E(\varphi) d\varphi. \quad (6)$$

The minus sign in Eq. (5) is due to the opposite energies of the Andreev bound states at negative and positive energies; their energies $\pm\langle E \rangle$ averaged over the phase

are also exactly opposite. This argument and additional comments are presented in Sec. VI of Supplemental Material in the case of a single band. Similar equations were obtained long ago in classical papers on Wannier-Stark theory (see for instance Ref. 42).

It is important to note that for two weakly coupled Wannier-Stark ladders, the average energy $\langle E \rangle$ depends on V . This corresponds to dressing each eigenstate in a given ladder by virtual transitions to the other ladder. These processes can be captured in a perturbative expansion in V . This is to be contrasted with Landau-Zener-Stückelberg transitions, which appear as tunneling processes between ladders, therefore giving contributions which are analytic functions of $1/V$ (see below). In Eqs. (4) and (5), only the first processes are taken into account, through the analytic dependence of $\langle E \rangle$ as a function of V .

The FWS-Andreev resonance energies defined by Eqs. (4) and (5) are shown by solid horizontal lines on top of the band structure of the extended Hamiltonian (see Fig. 3). Fig 3a shows two ladders with FWS-Andreev resonances being significantly “misaligned” in energy (tunneling is then essentially with the quasiparticle continua). Fig. 3b corresponds to FWS-Andreev resonances almost “aligned” in energy (with possibility of tunneling between the two Andreev resonances belonging to different ladders). In all cases, tunneling proceeds through a classically forbidden region, which has a length [in the auxiliary variable $l = (N_a - N_b)/2$] inverse proportional to the tilt (the tilt is proportional to bias voltage). The theory of tunnel effect states that tunneling decreases exponentially with the length of the barrier. Tunneling is thus exponentially small in the inverse of bias voltage. Tunneling between the FWS-Andreev resonances and the continua is consistent with the voltage-dependence of the FWS-Andreev line-width broadening, which will be evaluated numerically in Sec. III.

B. Three-terminal junctions

Now, remarks are provided on a generalization to three superconducting terminals connected to a single dot (see Fig. 1). In this case, the equilibrium Andreev bound states depend on the two phase variables φ_a and φ_b . With opposite bias voltages $\pm V$ on S_a and S_b (S_c being grounded), the time evolution of those phases is such that $\varphi_a(t) = \varphi_a(0) + 2eVt/\hbar$ and $\varphi_b(t) = \varphi_b(0) - 2eVt/\hbar$ (and $\varphi_c = 0$ is the reference phase). As mentioned in the Introduction, the quartet phase $\varphi_Q = \varphi_a(t) + \varphi_b(t) = \varphi_a(0) + \varphi_b(0)$ is static if $V_a + V_b = 0$, and the phase difference $\varphi_a(t) - \varphi_b(t)$ is winding in time: $\varphi_a(t) - \varphi_b(t) = 4eVt/\hbar$. The trajectories of the phases in the (φ_a, φ_b) plane are shown in Fig. 4 for $\varphi_Q = 0$ (green line) and for a generic $\varphi_Q \neq 0$ (red line). For the former, the gap between Andreev bound states closes at two opposite values of the phases, located in between $(0, 0)$ and (π, π) and, for the opposite phases, in between $(0, 0)$ and $(-\pi, -\pi)$

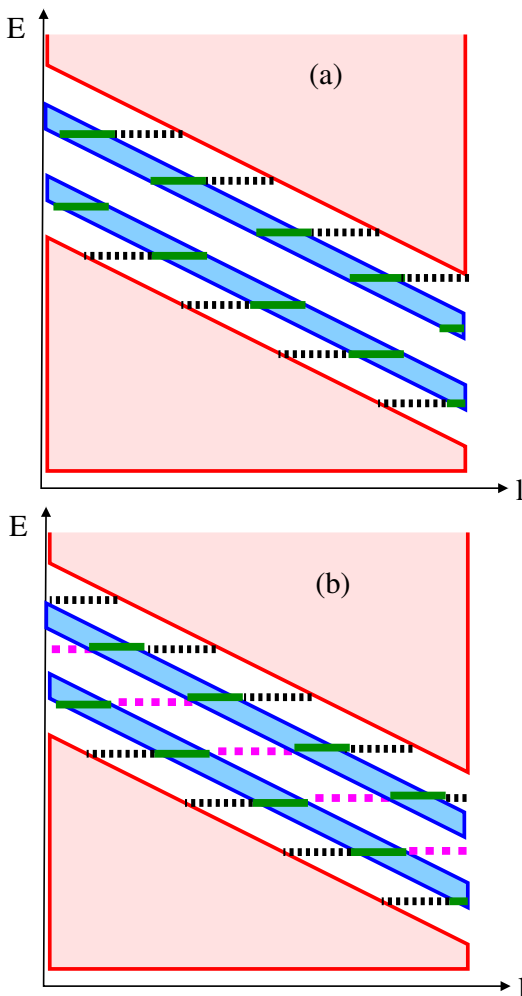


FIG. 3: *FWS-Andreev ladders*: The figure shows schematically the FWS-Andreev ladders for a two-terminal Josephson junction in the (l, E) plane, where the auxiliary variable $l = (N_a - N_b)/2$ is conjugate to the phase difference $\varphi_a - \varphi_b$. Panel a shows FWS-Andreev ladders with misaligned FWS-Andreev resonances (green solid lines). Tunneling is then essentially with the semi-infinite quasiparticle continua (dashed back lines). Panel b shows schematically aligned FWS-Andreev resonances, with also interband tunneling in this case. The energies of the FWS-Andreev resonances are given by Eqs. (4) and (5). The length of the solid lines shows the extent of the wave-functions along the axis of the auxiliary variable l . The wave-functions can be delocalized on both ladders in the case of aligned FWS-Andreev resonances, because of interband tunneling through the classically forbidden region (panel b). Interband tunneling produces energy level repulsion between hybridized FWS-Andreev resonances in this case.

(see Ref. 43). On the contrary, the gap between Andreev bound states does not close in the generic case $\varphi_Q \neq 0$ considered in the forthcoming Sec. III (red line in Fig. 4). The auxiliary variable $l = (N_a - N_b)/2$ is conjugate to the fast variable $\varphi_a - \varphi_b$. The FWS-Andreev viewpoint is identical to Fig. 3, but now this figure is also param-

eterized by the quartet phase φ_Q . Eqs. (4) and (5) still hold for three-terminals, where $\langle E \rangle$ is the average over $\varphi_a - \varphi_b$ of the energy of the upper bound state. For a three-terminal set-up, $\langle E \rangle$ is also parameterized by the quartet phase φ_Q .

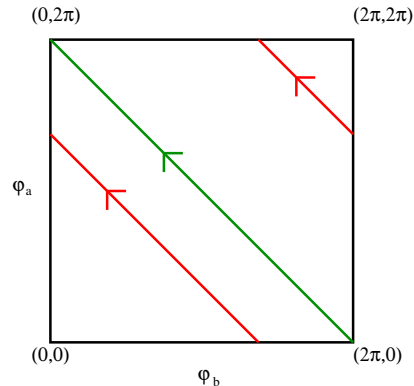


FIG. 4: The figure shows, for a three-terminal Josephson junction, the trajectories of the phases $(\varphi_a(t), \varphi_b(t))$ with a vanishingly small quartet phase $\varphi_Q = 0$ (green), and with a generic quartet phase $\varphi_Q \neq 0$ (red line). The time-dependence of the phases are given by $\varphi_{a,b}(t) = \varphi_{a,b}(0) \pm 2eVt/\hbar$, where opposite voltages $V_{a,b} = \pm V$ are applied on $S_{a,b}$ with respect to the grounded S_c .

C. Self-induced Rabi resonances

The first theoretical work³³ addressing phase-coherent three-terminal Josephson junctions coined those quartets and higher-order resonances as “self-induced Shapiro steps” appearing for rational ratios between bias voltages. Going now one step further, it is found here that, at fixed commensuration ratio $V_b/V_a = p/q$ (with p and q two integers), voltage-parameterized “self-induced Rabi resonances” are obtained between FWS-Andreev resonances belonging to different sub-bands. However, self-induced Rabi resonances are not specific to three superconducting terminals: on the contrary, similar Rabi resonances are expected also in a set-up consisting of two superconductors connected to a quantum dot. Three-terminal Josephson junctions at the quartet resonance offer the quartet phase as an additional control parameter.

Coming back to a three-terminal Josephson junction with $V_a = -V_b \equiv V$, it is deduced from Eqs. (4) and (5) that self-induced Rabi resonances appear at voltages

$$2eVj + \langle E \rangle = 2eVj' - \langle E \rangle, \quad (7)$$

with j and j' two integers. In the low voltage limit, a sequence of Rabi resonances at voltages

$$V_k = \frac{V_1}{k} \quad (8)$$

is expected, with k an integer, and $eV_1 = \lim_{V \rightarrow 0}(E)$. In the limit of small coupling $\Gamma/\Delta \ll 1$ between the dot and the superconducting leads, this leads to $eV_R \simeq \Gamma$. Tunneling between the dot and each of the superconducting electrodes is parameterized in a standard way by $\Gamma = J^2/W$, with J the corresponding hopping matrix element and W the band-width.

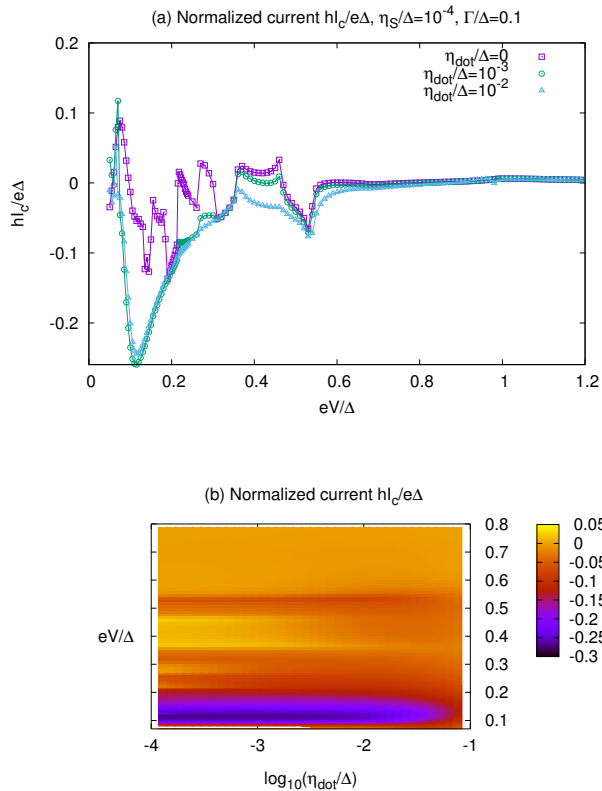


FIG. 5: Variations of the current I_c through lead S_c : Panel a shows the voltage dependence of the normalized current $hI_c/e\Delta$ as a function of normalized voltage eV/Δ for the values of η_{dot}/Δ indicated on the figure. Panel b shows $hI_c/e\Delta$ in the plane of the variables $(\log(\eta_{dot}/\Delta), eV/\Delta)$.

D. Generalized Dynes parameter η_{dot}

A finite bias voltage makes the FWS-Andreev resonances qualitatively different from Andreev resonances at equilibrium. For instance, MARs due to finite voltage contribute to the width of FWS-Andreev resonances. MARs produce only tiny relaxation at sufficiently low voltage (exponentially small in Δ/eV), thus indicating that FWS-Andreev ladders of resonances are robust against relaxation due to the coupling by MARs to the semi-infinite quasiparticle continua. However, if one wants to make experiments or to put this problem on a computer as it is done below, other mechanisms

for relaxation have to be taken into account, which will be dominant once MARs become too weak at low bias voltage. From the point of view of numerical calculations, relaxation is encoded in the Dynes parameter η_S in the superconductors. Electron-phonon scattering is a natural candidate for relaxation on the quantum dot (see also Sec. VIII of Supplemental Material). Once the Dynes parameter η_S has been introduced in the superconductors, then the generalized Dynes parameter η_{dot} has to be also included on the quantum dot, because of a question of internal consistency of the description (phonons operate both in the superconducting leads and on the quantum dot). It is then obvious that, for a resonant quantum dot, η_{dot} is much more efficient than η_S as a relaxation mechanism (See Sec. III for the numerical results and Sec. VIII in Supplemental Material for an explanation based on an analytical Green's function calculation). Transport theory with finite η_{dot} is more challenging than for $\eta_{dot} = 0$, but a mathematically exact solution for the current can be well obtained at finite η_{dot} (see Secs. I, II and III in Supplemental Material). The authors are aware that a finite η_{dot} is against recipes in the literature, and more especially against our previous work³⁵: The limit $\eta_{dot} = 0^+$ was taken, and, in practise, $\eta_{dot} = 0$ was implemented without questioning why $\eta_{dot} = 0$ is equivalent to $\eta_{dot} = 0^+$. The smoking gun that nontrivial physics is related to a finite $\eta_{dot} \neq 0$ is that adiabatic theorem breaks down severely for a three-terminal Josephson junction with two levels at energies $\pm\epsilon_0$ (in this case, the currents calculated with $\eta_{dot} = 0^+$ are not equal to those for $\eta_{dot} = 0$) (See Sec. IID of Supplemental Material). The situation is not so drastic for a single quantum dot having a level a zero energy: adiabatic theorem can well be demonstrated in this case (see Secs. I and II of Supplemental Material), which provides evidence that our previous calculations³⁵ for $\eta_{dot} = 0$ are mathematically correct in the sense that the currents take identical values for $\eta_{dot} = 0$ and $\eta_{dot} = 0^+$. However, our previous work³⁵ leaves open central questions such as those related to the speed of convergence of the current to its adiabatic limit value: The latter is found here to be exponentially small in Δ/V , which, in essence, is due to the emergence of those low-energy/long-time scales of interest here. Indeed, the characteristic η_{dot}^* for cross-over in the current to the adiabatic limit (corresponding $\eta_{dot} \ll \eta_{dot}^*$) receives the interpretation of the inverse of an intrinsic characteristic time scale.

On a more physical basis, some modes of the quantum dot are almost isolated from their environment, which explains long relaxation times. For instance, heat transport is expected to be very slow at low bias voltage for the set-up in Fig. 1, because the environment of the quantum dot consists of three BCS superconductors which do not propagate entropy over large distances (see the discussion in the concluding Sec. IVC). Supplemental Material offers large amount of technical details intended to unveil the theoretical framework behind the numerical results presented now.

III. NUMERICAL CALCULATIONS

The following calculations are carried out with a resonant quantum dot connected to three superconducting leads S_a , S_b and S_c biased at $V_{a,b} = \pm V$ and $V_c = 0$ respectively, in the presence of a generic finite value for the static quartet phase $\varphi_Q \neq 0$. The starting point is the Hamiltonian given in Appendix. The (Keldysh) Green's functions are calculated from the Dyson(-Keldysh) equations in extended space, and the currents are expressed in terms of the Dyson-Keldysh Green's function. The codes with $\eta_{dot} \neq 0$ are based on implementation of a self-consistency loop on the bare populations of the quantum dot. All numerical results presented below are obtained with recursive Green's functions in energy (see Refs. 44,45). Technical details on the principle of the codes are provided in Supplemental Material (see more especially Sec. III in Supplemental Material for a discussion of $\eta_{dot} \neq 0$).

The variations of current I_c through lead S_c are shown in Fig. 5 as a function of normalized voltage eV/Δ and normalized generalized Dynes parameter η_{dot}/Δ , for $\Gamma/\Delta = 0.1$. As mentioned above, the contact transparencies are parameterized by $\Gamma = J^2/W$, with J the hopping matrix element between the dot and the superconducting leads, and W the band-width. It was verified on a few examples that the following results are compatible with those obtained previously³⁴ for $\eta_{dot}/\Delta = 0$. A technical discussion is summarized in Secs. I, II and III in Supplemental Material, on how our calculations with a tiny $\eta_{dot}/\Delta = 0^+$ relate to those with $\eta_{dot}/\Delta = 0$ in our previous work³⁴. The variations of I_c with eV/Δ (see Fig. 5a) look much smoother than those obtained for $\eta_{dot}/\Delta = 0$ once a tiny $\eta_{dot}/\Delta = 10^{-3} \div 10^{-2}$ is included. The currents are evaluated according to the self-consistent procedure presented in Sec. III of Supplemental Material. The first of the self-induced Rabi resonances [see Eq. (8) with $k = 1$] is in agreement with the maximum at $eV/\Delta \simeq 0.1$ in the voltage dependence of the normalized current $hI_c/e\Delta$ (see Fig. 5 for $\eta_{dot}/\Delta = 10^{-3}$, 10^{-2} and $\Gamma/\Delta = 0.1$). This Rabi resonance was predicted in Sec. II at $eV_R = \langle E \rangle \simeq \Gamma$ if $\Gamma/\Delta \ll 1$. Fig. 5 does not fully match this condition of tunnel contacts, because $\Gamma/\Delta = 0.1$ is not a very small number. A resonance appears in Fig. 5a at voltage slightly larger than $V_R/\Delta = 0.1$, and that is also visible in Fig. 5b, featuring the normalized current $hI_c/e\Delta$ (in color-scale) in the plane of parameters $(\log(\eta_{dot}/\Delta), eV/\Delta)$. To conclude the discussion of those first numerical observations, ultra-sensitivity on a tiny η_{dot}/Δ (see Fig. 5) is a first numerical evidence for emergence of small-energy/long-time scales: a small cross-over value η_{dot}^* for convergence towards adiabatic limit in $I_c(\log(\eta_{dot}/\Delta))$ implies a long time \hbar/η_{dot}^* . In addition, it is found here that the voltage scale V_R controls the voltage-dependence of the current once a small η_{dot}/Δ is included.

Now that one of the Rabi resonances has been confirmed, further numerical evidence is provided for the

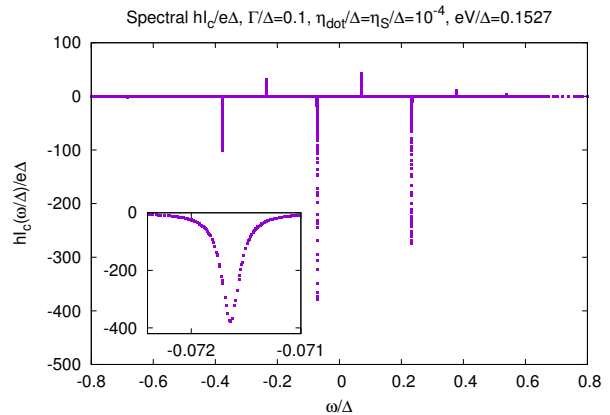


FIG. 6: *Spectral current I_c* : The figure shows the frequency ω dependence of the normalized spectral current $hI_c(\omega/\Delta)/e\Delta$. The insert (with the same axis labels as the main panel) shows the same quantity in the vicinity of a specific resonance.

fully replicated Floquet spectrum, and, more precisely, for the double FWS-Andreev ladder. A first possibility for visualizing the two FWS-Andreev ladders (see Fig. 6) is to plot the spectral current as a function of energy. This quantity measures the contribution to the total current of FWS states at a given energy ω so that the dc current is obtained as the integral over ω of the spectral current. Fig. 6 reveals sharp resonances with alternating signs, corresponding to the two alternating FWS-Andreev ladders carrying opposite currents, as for Andreev bound states at equilibrium. Fig. 6 confirms the generalization to nonequilibrium of Andreev bound states carrying opposite currents. The insert of Fig. 6 enlarges a selected resonance, which reveals the smallness of its width in energy, due to the weakness of the equilibrating mechanisms. The data-points shown in Fig. 6 correspond to the raw ones, evaluated with an adaptive algorithm for integration over energy ω (the data for Fig. 6 are part of those for Fig. 5b).

The voltage dependence of the FWS-Andreev resonance energies [see Eqs. (4) and (5)] is discussed now. Recursive calculations are implemented to calculate numerically the Floquet-Lippmann-Schwinger wave-function (see Sec. V in Supplemental Material). Technically, the FWS-Andreev ladders are obtained from the maxima over the energy $E_{k,c}$ of the maximum over the auxiliary variable $l = (N_a - N_b)/2$ of the Floquet-Lippmann-Schwinger wave-function. Eqs. (4) and (5) can be written as

$$\frac{E_j}{eV} = 2j + \frac{\langle E \rangle}{\Delta} \times \frac{\Delta}{eV} \quad (9)$$

$$\frac{E'_{j'}}{eV} = 2j' - \frac{\langle E \rangle}{\Delta} \times \frac{\Delta}{eV}. \quad (10)$$

Fig. 7 shows plots inspired by Ref. 42, in which the x -axis is Δ/eV and the y -axis is $E_{k,c}/eV$ ($E_{k,c}$ is the energy of the quasiparticle injected at wave-vector k into lead S_c). Fig. 7a (for $\Gamma/\Delta = 0.1$) and Fig. 7b

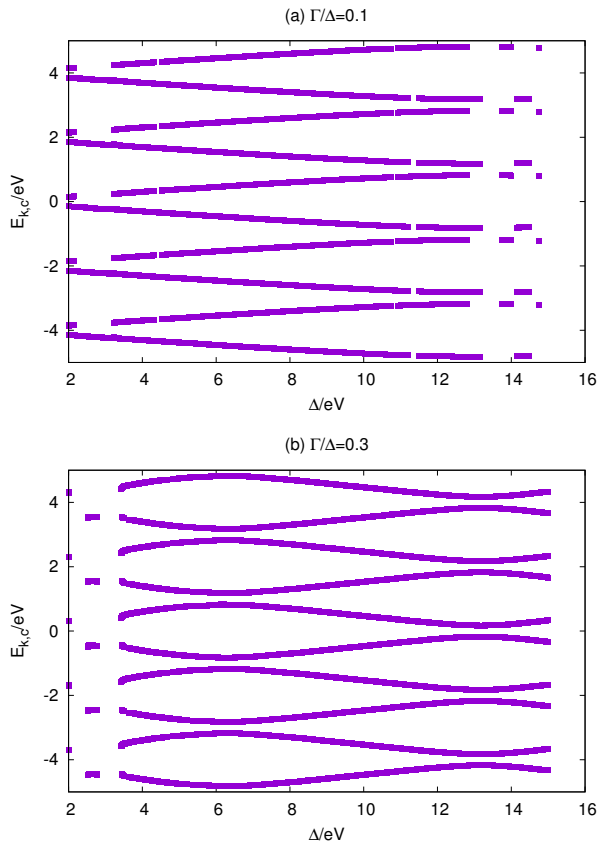


FIG. 7: *Inverse voltage dependence of the FWS-Andreev resonances*: The figure shows the inverse voltage dependence of $E_{k,c}/eV$, the Floquet-Lippmann-Schwinger energy parameter divided by voltage. Panel a corresponds to $\Gamma/\Delta = 0.1$, and panel b to $\Gamma/\Delta = 0.3$.

(for $\Gamma/\Delta = 0.3$) reveal two ladders of Andreev resonances compatible with Eqs. (9) and (10). A ladder with positive slope $\langle E \rangle/\Delta$ alternates with the other one with negative slope $-\langle E \rangle/\Delta$. In addition, numerical evidence for repulsion between FWS-Andreev resonances is obtained at the crossing points, due to Landau-Zener-Stückelberg transitions. A qualitative agreement is obtained in the voltage-dependence of the normalized current $hI_c/e\Delta$, and of the spectrum of FWS-Andreev resonances (obtained from the Floquet wave-function; see Fig. 7). Namely, the current is controlled by eV_R/Δ slightly above $eV_R/\Delta \simeq \Delta/10$ while the avoided crossings are at $\Delta/eV_1 \simeq 14$. Quantitatively, the voltage V_1 is clearly smaller than V_R . A first explanation is that the current I_c does not depend only on the resonance spectrum but also on the full FWS-Andreev wave-function and on the occupation of the FWS-Andreev resonances. On the other hand, more trivially, no obvious reason can be advocated of why perfect quantitative agreement is expected on cross-over values of different quantities calculated in different manners. Further investigations involve recalculating the current I_c with FWS-Andreev

wave-functions, but this goes beyond the scope of the present paper.

The paper deals solely with the current I_c through lead S_c (see Fig. 1), which corresponds to a pair current due to the quartet or multipair mechanism, with vanishingly small quasiparticle component due to MARs. All contacts between the quantum dot and the superconducting leads have identical transparency and, together with the assumption of particle-hole symmetry, it can be demonstrated³⁴ that the corresponding I_c is due solely to correlations among Cooper pairs, without quasiparticles. It is thus acceptable to address a link between equilibrium and nonequilibrium DC-superflows, without the contribution of MARs in the current, except for the contribution of those in the line-width broadenings.

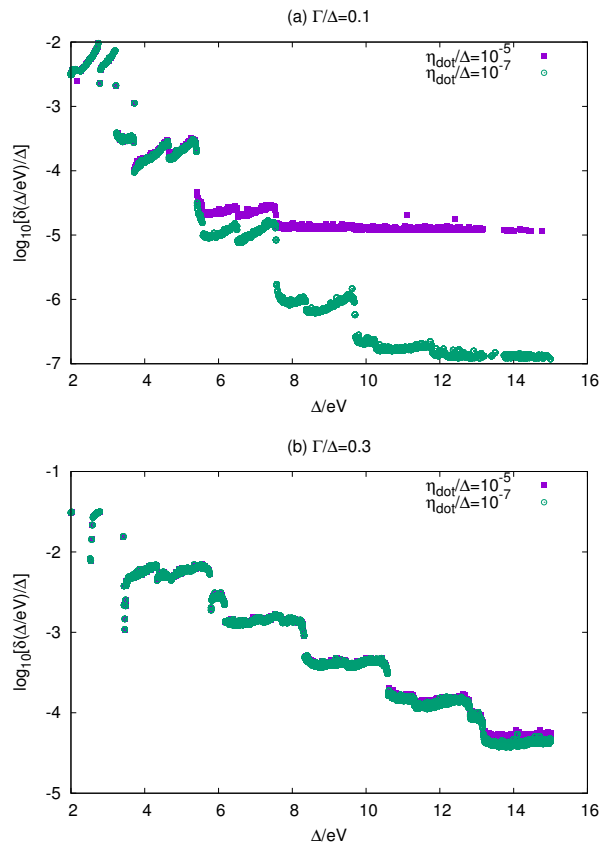


FIG. 8: *Inverse voltage dependence of the line-width broadening*: The figure shows the variations of the logarithm of the normalized line-width broadening δ/Δ of the FWS-Andreev resonances as a function of the normalized inverse voltage Δ/eV , for the values of η_{dot}/Δ shown on the figure. Panel a corresponds to $\Gamma/\Delta = 0.1$ and panel b to $\Gamma/\Delta = 0.3$.

As discussed above, the equilibrating coupling to the semi-infinite quasiparticle continua is exponentially small in the inverse of voltage: In the FWS-Andreev viewpoint, this coupling is due to tunneling from the FWS-Andreev ladders to the continua, through a classically forbidden region of length inverse proportional to the bias voltage (see Sec. II). On the other hand, tunneling through

the classically forbidden region proceeds from MARs. Each elementary electron-hole or hole-electron process increases or reduces by unity the value $l = (N_a - N_b)/2$ of the auxiliary variable introduced in the preceding Sec. II and in Sec. VI of Supplemental Material. Thus, the FWS-Andreev viewpoint suggests the appearance of step-like variations for the logarithm δ/Δ , the normalized line-width broadening of FWS-Andreev resonances as a function of inverse bias voltage. The voltage-dependence of δ/Δ is thus expected to share similarities with that of the DC-current of MARs in a superconducting quantum point contact^{44,46}.

Those expectations for the normalized FWS-Andreev line-width broadening δ/Δ are fully confirmed by the numerical results shown in Fig. 8a (for $\Gamma/\Delta = 0.1$) and Fig. 8b (for $\Gamma/\Delta = 0.3$). The values of $\delta(\Delta/eV)/\Delta$ are plotted in Fig. 8a and in Fig. 8b as a function of inverse normalized voltage Δ/eV . The overall behavior for the envelope of $\delta(\Delta/eV)/\Delta$ is the following: $\log(\delta(\Delta/eV)/\Delta) \sim -\Delta/eV$, and distinguishing features of regularly spaced steps delimited by MAR thresholds are clearly identified in the variations of $\log[\delta(\Delta/eV)]$. The corresponding voltages are $eV_n = \Delta/2n$, with $n = 3, 4, 5$. The comparison between $\eta_{dot}/\Delta = 10^{-5}$ and $\eta_{dot}/\Delta = 10^{-7}$ (see Figs. 8a and b) shows that, for $\Gamma/\Delta = 0.1$, the low-voltage (large Δ/eV) normalized line-width broadening $\delta(\Delta/eV)/\Delta$ is strongly sensitive on relaxation, through the normalized Dynes parameter η_{dot}/Δ . The dominant contribution to δ/Δ originates from η_{dot}/Δ at low eV/Δ and Γ/Δ , which is in agreement with the forthcoming discussion on Fig. 9. The sensitivity on η_{dot}/Δ is much weaker for the larger value $\Gamma/\Delta = 0.3$, because the coupling to the quasiparticle continua is much larger for $\Gamma/\Delta = 0.3$ than for $\Gamma/\Delta = 0.1$. The FWS-Andreev avoided crossings in Figs. 7a and b do not correlate at all with the steps in Figs. 8a and b. This shows that, as it is discussed above, it is MARs (and not the avoided crossings in themselves) which are at the origin of the steps in $\log(\delta(\Delta/eV))$.

Fig. 9 shows for the set-up in Fig. 1 the variations of the normalized current $hI_c/e\Delta$ through lead S_c at fixed voltage V , as a function of $\log(\eta_{dot}/\Delta)$. The different curves correspond to Dynes parameters $\eta_S/\Delta = 10^{-6}, 10^{-5}, 10^{-4}$. The current becomes almost independent on η_{dot}/Δ and η_S/Δ if those Dynes parameter ratios are sufficiently small. In this regime, the current takes its adiabatic limit value (corresponding to $\eta_{dot}/\Delta = 0^+$ and $\eta_S/\Delta = 0^+$; see the discussion in Secs. I and II of Supplemental Material). Considering for simplicity the limit $\eta_S = 0^+$, the characteristic cross-over value η_{dot}^*/Δ of the Dynes parameter η_{dot}/Δ is defined practically as the inflection point in the variations of $I_c(\log(\eta_{dot}/\Delta))$ (see Fig. 9). The equilibration time \hbar/η_{dot}^* corresponds to the characteristic time for connecting by MARs the low-energy quantum dot degrees of freedom to the semi-infinite quasiparticle continua above the gaps. Crossing-over between MAR-dominated equilibration ($\eta_{dot} \ll \eta_{dot}^*$) and electron-phonon-dominated equi-

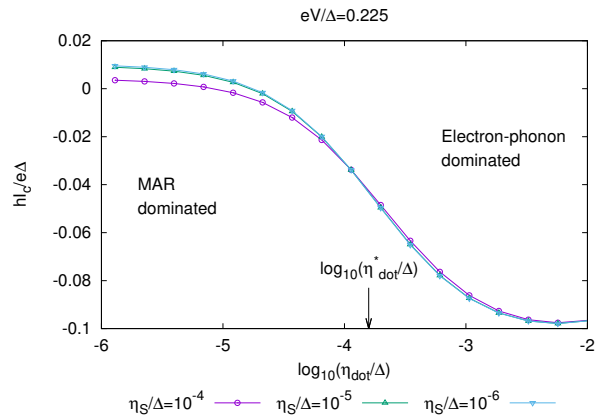


FIG. 9: *Illustration of the two regimes:* The figure shows the $\log(\eta_{dot}/\Delta)$ -dependence of the normalized current $hI_c/e\Delta$, for the set-up in Fig. 1, and for the values of η_S/Δ shown on the figure, with $\Gamma/\Delta = 0.1$ and with a generic finite value for the quartet phase. The data-points with $\eta_S/\Delta = 10^{-5}$ almost match those for $\eta_S/\Delta = 10^{-6}$, which is evidence for convergence towards adiabatic limit as η_{dot}/Δ and η_S/Δ are reduced. The variable η_{dot}^* is defined as the value of η_{dot} at which the inflection point appears on those curves. The characteristic cross-over values \hbar/η_{dot}^* and \hbar/η_S^* receive the interpretation of characteristic times for equilibration with the semi-infinite quasiparticle continua above the gaps via MARs. If $\eta_S = 0^+$, the characteristic cross-over value η_{dot}^* separates between two regimes: MAR-dominated equilibration for $\eta_{dot} \ll \eta_{dot}^*$, and electron-phonon-dominated for $\eta_{dot} \gg \eta_{dot}^*$. The experimental values for \hbar/η_{dot} and \hbar/η_S in a given sample are to be compared with the characteristic times \hbar/η_{dot}^* and \hbar/η_S^* in order to determine the dominant equilibration mechanism.

libration ($\eta_{dot} \gg \eta_{dot}^*$) changes the sign of I_c in Fig. 9. The nature of the dominant equilibrating mechanism can thus produce important qualitative changes in the value of physical observables such as the current I_c . Thus, we discuss here the possibility of important deviations with respect to our previous work³⁴, in which $\eta_{dot} = \eta_S = 0$. The smallness of η_{dot}^*/Δ makes it plausible that, depending on the experimental values for the Dynes parameters and for bias voltages, the regime $\eta_{dot} \gg \eta_{dot}^*$ can be more relevant to experiments⁶ than the limit $\eta_{dot} = 0$ considered previously³⁴. A planned project related to a comparison of this theory with the Weizmann group experimental data⁶ is mentioned in the concluding Sec. IV B.

The normalized inverse voltage- Δ/eV dependence of η_{dot}^* is presented in Fig. 10, in the limit $\eta_S = 0^+$. The characteristic cross-over value η_{dot}^*/Δ is determined from the inflection point in $I_c(\log(\eta_{dot}/\Delta))$ (see Fig. 9). The change at $\Delta/eV \simeq 12$ is in between $\Delta/eV_R \simeq 10$ [V_R is the voltage associated to the resonance seen on Fig. 5] and $\Delta/eV_1 \simeq 14$ [V_1 is the voltage at which the avoided crossing occurs in Fig. 7 and defined in Eq. (8)]. Considering first the high-voltage regime ($\Delta/eV \lesssim \Delta/eV_R$), the overall voltage dependence of the envelope of $\log(\eta_{dot}^*/\Delta)$ is compatible with the scaling $\log(\eta_{dot}^*/\Delta) \sim -\Delta/eV$ (see

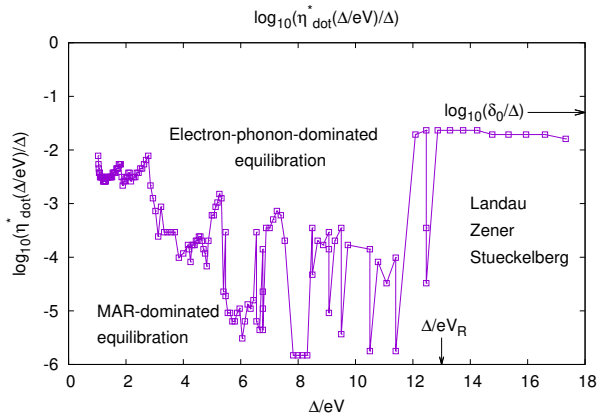


FIG. 10: *Inverse voltage dependence of η_{dot}^*/Δ* : The figure shows η_{dot}^*/Δ as a function of Δ/eV for the set-up in Fig. 1, and for $\Gamma/\Delta = 0.1$. The value of η_{dot}^*/Δ is determined from the inflection points of $I_c(\eta_{dot}/\Delta)$ for all values of voltage, for the same data as in Fig. 5b. The arrows on the x axis indicates V_R [see Eq. (8)]. The arrow on the y axis indicates δ_0 , the splitting between FWS-Andreev ladders at the avoided crossing (see Fig. 7).

Fig. 10), which coincides with the same overall scaling for the spectral quantity $\log(\delta/\Delta)$ (see Fig. 8a). The nonmonotonous behavior of the voltage dependence of η_{dot}^*/Δ (see Fig. 10) is compatible with a strong enhancement of $\log(\eta_{dot}^*/\Delta)$ at the MAR thresholds, such as the first terms in the series $eV_n = \Delta/(2n + 1)$, with $n = 1, 2, 3$. It is expected that coupling the quantum dot by MARs to the gap edge singularities of one of three superconductors is like resonantly coupling the quantum dot to a normal bath, producing strong equilibration at the specific voltages of the MAR thresholds. On the other hand, the value of $\log(\eta_{dot}^*/\Delta)$ is much larger if $\Delta/eV \gtrsim \Delta/eV_R$, which matches the onset of coherence between the two FWS-Andreev ladders. The value of η_{dot}^* for $\Delta/eV \gtrsim \Delta/eV_R$ is compatible with δ_0 , the splitting between FWS-Andreev resonances (see Fig. 7). It was mentioned above that the interpretation of Fig. 5 (regarding the comparison between $\eta_{dot}/\Delta = 0$ and $\eta_{dot}/\Delta = 10^{-3}$) implies that very low characteristic scales of η_{dot}/Δ appear in $I_c(\log(\eta_{dot}/\Delta))$ at low bias voltage, even if $V \lesssim V_R$. This implies multiple values for η_{dot}^*/Δ if $V \lesssim V_R$, which are hidden from Fig. 10 in order to keep the presentation of this cross-over diagram as simple as possible. Obvious difficulties arise in the numerics to detect with an adaptive integration algorithm all of the FWS-Andreev resonances contributing significantly to the spectral current at low V/Δ and very low- η_{dot}/Δ , because the width of those resonance is tiny in this parameter range. The raw data (which are not presented here) for the variations of $I_c(\log(\eta_{dot}/\Delta))$ with $\log(\eta_{dot}/\Delta)$ were carefully inspected in voltage window $V \lesssim V_R$. Inflection points appear in $I_c(\log(\eta_{dot}/\Delta))$ at very low η_{dot}/Δ (the detected inflection points are typically in the interval $-6 \lesssim \log(\eta_{dot}/\Delta) \lesssim -4.5$). An over-

all trend to complex variations of $I_c(\log(\eta_{dot}/\Delta), eV/\Delta)$ is obtained in addition in the same voltage window. Qualitatively, the behavior of η_{dot}^*/Δ correlates with spectral properties such as the FWS-Andreev line-width broadening δ due to the coupling to the semi-infinite quasiparticle continua of the FWS-Andreev ladders of resonances (see Fig. 8), because both quantities are exponentially small in Δ/eV . However, quantitatively, it is not possible to determine to which extent the onset of the Landau-Zener-Stückelberg region of the cross-over diagram upon reducing V/Δ is closer to V_R than to V_1 . The conclusion is thus that it is remarkable that qualitatively, the low-energy scales in the current relate to those in FWS-Andreev spectrum. However, the correspondence is not quantitative, for the obvious reasons which were already mentioned above.

IV. CONCLUSIONS AND DISCUSSION

A. Conclusions

At equilibrium, the supercurrent is calculated solely in terms of to the spectrum of Andreev bound states once the states at negative energy have received their equilibrium occupation numbers at zero temperature. A less demanding relation between the current I_c through lead S_c and spectral properties was addressed in the more complex situation of relaxation due to the generalized Dynes parameter η_{dot} (encoding relaxation due to the coupling to phonons), and of a coupling by MARs to the semi-infinite quasiparticle continua. More precisely, it was demonstrated numerically that, qualitatively, the characteristic low-energy scales in the supercurrent I_c through lead S_c are related to those in the FWS-Andreev spectrum of resonances, because those have similar voltage-dependence. Three low-energy (long-time) scales emerge in those numerical calculations based on Keldysh Green's functions and on the Floquet-Lippmann-Schwinger dressing algorithm: First, already for a single FWS band, the spectral line-width broadening δ of FWS resonances is exponentially small in Δ/eV (with Δ the superconducting gap), due to the coupling by multiple Andreev reflections to the semi-infinite quasiparticle continua above the gaps. Second, the degeneracy of the FWS-Andreev two-level system is lifted by an amount δ_0 at avoided crossings. Third, the cross-over value η^* of the Dynes parameter η is related to the speed of convergence of the current towards adiabaticity in the limit $\eta \rightarrow 0^+$.

The qualitative correspondence between transport and spectral properties is however not quantitative, which is maybe not unexpected. In addition, the current I_c also couples to the FWS-Andreev wave-functions and to the populations of the FWS-Andreev ladders of resonances. Given the complexity of the set-up, it is remarkable that simple ideas such as a weak version of this relation between transport and the spectrum can be used to understand qualitatively the numerical calculations of the

characteristic low-energy/long time scales in the current I_c . It is within the achievements of the Keldysh dressing algorithm to obtain exact numerical values for the currents in the set-up of interest here. However, it is not within the scope of the Keldysh algorithm to provide by itself simple intuitive physical pictures. A full solution of the FWS-Andreev viewpoint (including calculation of the wave-functions and populations) is more promising to obtain simple physical explanations. The present paper is a first step along this roadmap.

Cavity quantum electrodynamics experiments are promising to perform the spectroscopy of the FWS-Andreev ladders of resonances (see for instance the recent Ref. 47). At present time, no obvious reason can be advocated on why the nonequilibrium FWS-Andreev two-level system should show experimental relaxation times much larger than that of the equilibrium Andreev two-level system^{13,14}. However, further studies are required in order to determine whether quasiparticle poisoning can be reduced by the applied bias voltage. At present stage, the best is probably to make the experiment without prejudice.

It was found that the normalized voltage- V/Δ dependence of the normalized line-width broadening $\delta(eV/\Delta)/\Delta$ of FWS-Andreev resonances is exponentially small in Δ/eV , which is the expected behavior: in the FWS-Andreev viewpoint, tunneling between the continua and FWS-Andreev ladders proceeds through a classically forbidden region of length proportional to Δ/eV . In addition, the normalized voltage- V/Δ dependence of the cross-over normalized Dynes parameters $\eta_{dot}^*(V/\Delta)/\Delta$ was evaluated, which is in the first place a quantity of physical interest. In the absence of coupling between the two FWS-Andreev ladders at voltage $V \gtrsim V_R$, the cross-over normalized Dynes parameter $\eta_{dot}^*(V/\Delta)/\Delta$ corresponds to the inverse of the characteristic time scale for connecting by MARs the low-energy quantum dot degrees of freedom with the quasiparticle semi-infinite continua above the gaps. Thus, \hbar/η_{dot}^* is the characteristic time scale for equilibration with those quasiparticle continua if $V \gtrsim V_R$. The characteristic time \hbar/η_{dot}^* is of order $\hbar/\eta_{dot}^* \sim 1/\delta_0$ if $V \lesssim V_R$, where δ_0 is the splitting of the FWS-Andreev two-level system. In addition, η_{dot}^* is multiply defined if $eV \lesssim V_R$, and much lower characteristic η_{dot}^* emerge for $V \lesssim V_R$, with complex behavior of the related $I_c(\eta_{dot}^*/\Delta, V/\Delta)$.

B. Perspectives on the recent Weizmann group experiment⁶

The interpretation of the Weizmann group cross-correlation experiment⁶ is the following: A train of quartets transmitted from S_c to (S_a, S_b) is produced, followed by another train from (S_a, S_b) to S_c , and so on. This is reminiscent of thermal effects on the noise of a two-terminal point contact at equilibrium but there, it is the quantum coherent Landau-Zener-Stückelberg

(LZS) transitions (instead of incoherent thermally activated processes) which change randomly the direction of the quartet superflow. In the experimental Ref. 6, temperature is sufficiently low that the thermally activated processes are negligibly small in the noise cross-correlations (those are exponentially suppressed in the ratio between the BCS gap and the temperature). A noticeable difference between LZS transitions and thermal activation lies in full quantum coherence for the former, with possible correlations among huge numbers of Cooper pairs. In addition, in realistic situations, a temperature dependence of the generalized Dynes parameter could appear, as it is expected for inelastic effects. The line-width broadening due to the continua is exponentially small in the inverse of voltage, and the generalized Dynes parameter is exponentially small in the inverse of temperature. A cross-over temperature comparable to voltage is thus expected.

The present results and those of the Weizmann group⁶ share intriguing similarities: The time scale $\sim \hbar/\delta$ (the inverse of the FWS-Andreev line-width broadening) is possibly related to the overall coherence time for the absolute value of the current in this picture of LZS transitions. The scale $\sim \hbar/\delta_0$ (the inverse of the level degeneracy at a FWS-Andreev avoided crossing) is possibly related to the much shorter coherence time for the sign of the current. The energy scale η^* controls whether equilibration is due to the coupling to the quasiparticle continua (for $\eta \lesssim \eta^*$) or to inelastic electron-phonon scattering (for $\eta \gtrsim \eta^*$). Further calculations for the voltage and quartet phase sensitivity of the cross-correlations are required to determine the nature of the dominant equilibrating mechanism in the Weizmann group experiment⁶. In addition, gain of realism can be obtained by discussing finite temperature effect on the quasiparticle populations, and by treating double (instead of single) quantum dots.

The recent experimental results of the Weizmann group⁶ were compared in the same preprint to Keldysh Green's function calculations for the noise. The calculated current cross-correlations⁶ provide evidence for resonance in DC-current and cross-correlations as the quartet phase $\varphi_Q = \varphi_a + \varphi_b - 2\varphi_c$ is varied at fixed voltage $V \equiv V_a = -V_b$. This resonance parameterized by φ_Q is strongly sensitive on the value of the Dynes parameter ratio η_S/Δ : the cross-correlation signal varies by one order of magnitude as η_S/Δ is changed in the range $\eta_S/\Delta = 10^{-6} \div 10^{-3}$. This ultra-sensitivity of current cross-correlations on small values of the Dynes parameters is puzzling, especially with respect to what has been found here regarding the behavior of the current as a function of η_{dot} . This is why it would be also of interest to introduce η_{dot} in cross-correlation calculations, and to calculate the cross-correlations for η_{dot}/Δ smaller or larger than η_{dot}^*/Δ . The first question to be asked is probably whether the same inverse time scale \hbar/η_{dot}^* controls the current and the noise cross-correlations. Comparing with the experimental data of the Weizmann group⁶ may then provide useful information on the issue of whether

the quantum dot degrees of freedom are equilibrated with the quasiparticle continua in this experiment. This may be all the more interesting in view of the perspective on thermodynamics discussed now.

C. Perspective on quantum thermodynamics

Final remarks are presented now, in connection with a perspective on quantum thermodynamics in three-terminal Josephson junctions at the quartet resonance. A limit can be worked out analytically in which quasiparticles on the quantum dot never reach equilibration: the infinite gap limit. Coupling solely to superconducting condensates does not allow for propagation of entropy (because, in the infinite gap limit, each superconducting lead has the condensate as a single state, and a vanishingly small entropy). A small energy scale is expected in the presence of a finite gap and small η_S/Δ or η_{dot}/Δ , related to the interplay with the finite line-width broadening of FWS-Andreev resonances due to the coupling to quasiparticle continua above the gaps. Future evaluations of the heat current in a three-terminal Josephson junction biased in the quartet voltage configuration can thus bring informations complementary to those presented above.

To conclude, those three-terminal Josephson junctions can be viewed as prototypical examples of “half-open systems”. Those systems share features of open systems (for example: extended quasiparticle states above the gaps, finite current due to bias voltages on the leads) with the apparently contradicting features of closed system (for example: strong confinement of the quantum dot degrees

of freedom, poor equilibration, sharp Andreev resonances in the Floquet spectrum).

Acknowledgments

The authors acknowledge support from ANR Nanoquartets 12-BS-10-007-04. The authors thank the CRIANN in Rouen for use of its computing facilities. Part of the numerical calculations were also performed on the local computing facilities of Institut Néel in Grenoble. R.M. acknowledges fruitful discussions with Denis Feinberg, especially on the infinite-gap limit. R.M. thanks Jean Christian Anglès d’Auriac for having provided useful advice with daily numerics. R.M. and B.D. thank Didier Mayou for useful remarks on phonons in connection with Ref. 49. R.M. acknowledges stimulating discussions on thermodynamics with Alexia Affèves and Géraldine Haack. R.M. thanks the “Fondation Nanosciences” in Grenoble for financial support and useful discussions in the framework of Yuli Nazarov’s Chair of Excellence. R.M. thanks his collaborators from the Weizmann Institute: Yuval Cohen, Yonathan Ronen, Hadas Shtrickman and Moty Heiblum. R.M. wishes to express special thanks to Denis Basko for in-depth reading of a previous version of the manuscript, and for useful suggestions in connection with his recent solution⁵⁰ of a related time-dependent problem¹⁰. R.M. and B.D. thank Pascal Degiovanni for his previous collaboration on a related topic⁴⁸. Finally, R.M., J.G.C. and B.D. thank Jean-Jacques Préjean for his warm hospitality at the time where those ideas emerged, and for useful comments on the manuscript.

-
- ¹ S. B. Kaplan, C. C. Chi, D. N. Langenberg, J. J. Chang, S. Jafarey, and D. J. Scalapino, *Quasiparticle and phonon lifetimes in superconductors*, Phys. Rev. B **14**, 4854 (1976).
- ² R. C. Dynes, V. Narayanamurti, and J. P. Garno, *Direct measurement of quasiparticle-lifetime broadening in a strong-coupled superconductor*, Phys. Rev. Lett. **41**, 1509 (1978);
- ³ D. Averin and H.T. Imam, *Supercurrent noise in quantum point contacts*, Phys. Rev. Lett. **76**, 3814 (1996).
- ⁴ A. Martín-Rodero, A. Levy Yeyati, and F. J. García-Vidal, *Thermal noise in superconducting quantum point contacts*, Phys. Rev. B **53**, R8891(R) (1996).
- ⁵ B. Dassonneville, M. Ferrier, S. Guéron and H. Bouchiat, *Dissipation and supercurrent fluctuations in a diffusive normal-metal-superconductor ring*, Phys. Rev. Lett. **110**, 217001 (2013).
- ⁶ Y. Cohen, Y. Ronen, J.-H. Kang, M. Heiblum, D. Feinberg, R. Mélin, H. Shtrickman, *Non-local supercurrent of quartets in a three-terminal Josephson junction*, arXiv:1606.08436 (2016).
- ⁷ J.P. Pekola, V. F. Maisi, S. Kafanov, N. Chekurov, A. Kemppinen, Yu. A. Pashkin, O.-P. Saira, M. Möttönen, and J. S. Tsai, *Environment-assisted tunneling as an origin of the Dynes density of states*, Phys. Rev. Lett. **105**, 026803 (2010).
- ⁸ O.-P. Saira, A. Kemppinen, V. F. Maisi, and J. P. Pekola, *Vanishing quasiparticle density in a hybrid Al/Cu/Al single-electron transistor*, Phys. Rev. B **85**, 012504 (2012).
- ⁹ D. M. T. van Zanten, F. Balestro, H. Courtois, and C. B. Winkelmann, *Probing hybridization of a single energy level coupled to superconducting leads*, Phys. Rev. B **92**, 184501 (2015).
- ¹⁰ D.M.T. van Zanten, D.M. Basko, I.M. Khaymovich, J.P. Pekola, H. Courtois, and C. B. Winkelmann, *Single Quantum Level Electron Turnstile*, Phys. Rev. Lett. **116**, 166801 (2016).
- ¹¹ R.-P. Riwar, M. Houzet, J.S. Meyer and Y.V. Nazarov, *Control of Andreev bound state population and related charge-imbalance effect*, J. Phys.: Condens. Matter **27**, 095701 (2015).
- ¹² R.-P. Riwar, A. Hosseinkhani, L. D. Burkhardt, Y. Y. Gao, R. J. Schoelkopf, L. I. Glazman, G. Catelani, *Normal-metal quasiparticle traps for superconducting qubits*, Phys. Rev. B **94**, 104516 (2016).
- ¹³ L. Bretheau, Ç.Ö. Girit, H. Pothier, D. Esteve and C. Urbina, *Exciting Andreev pairs in a superconducting*

- atomic contact, *Nature* **499**, 7458 (2013) 312
- ¹⁴ C. Janvier, L. Tosi, L. Bretheau, Ç.Ö. Girit, M. Stern, P. Bertet, P. Joyez, D. Vion, D. Esteve, M.F. Goffman, H. Pothier and C. Urbina, *Coherent manipulation of Andreev states in superconducting atomic contacts*, *Science* **349** (6253), 1199 (2015).
 - ¹⁵ A. Freyn, B. Douçot, D. Feinberg, and R. Mélin, *Production of nonlocal quartets and phase-sensitive entanglement in a superconducting beam splitter*, *Phys. Rev. Lett.* **106**, 257005 (2011).
 - ¹⁶ R.-P. Riwar, M. Houzet, J.S. Meyer and Y.V. Nazarov, *Multi-terminal Josephson junctions as topological materials*, *Nature Communications* **7**, 11167 (2016).
 - ¹⁷ A. H. Pfeffer, J. E. Duvauchelle, H. Courtois, R. Mélin, D. Feinberg, and F. Lefloch, *Subgap structure in the conductance of a three-terminal Josephson junction*, *Phys. Rev. B* **90**, 075401 (2014).
 - ¹⁸ D. Beckmann, H. B. Weber, and H. v. Löhneysen, *Evidence for Crossed Andreev reflection in superconductor-ferromagnet hybrid structures*, *Phys. Rev. Lett.* **93**, 197003 (2004).
 - ¹⁹ S. Russo, M. Kroug, T. M. Klapwijk, and A. F. Morpurgo, *Experimental Observation of bias-dependent nonlocal Andreev reflection*, *Phys. Rev. Lett.* **95**, 027002 (2005).
 - ²⁰ P. Cadden-Zimansky and V. Chandrasekhar, *Nonlocal correlations in normal-metal superconducting systems*, *Phys. Rev. Lett.* **97**, 237003 (2006).
 - ²¹ L.G. Herrmann, F. Portier, P. Roche, A. Levy Yeyati, T. Kontos and C. Strunk, *Carbon nanotubes as Cooper pair beam splitters*, *Phys. Rev. Lett.* **104**, 026801 (2010).
 - ²² L. Hofstetter, S. Csonka, J. Nygård and C. Schönberger, *Cooper pair splitter realized in a two-quantum-dot Y-junction*, *Nature* **461**, 960 (2009).
 - ²³ A. Das, Y. Ronen, M. Heiblum, D. Mahalu, A.V. Kretinin and H. Shtrikman, *High-efficiency Cooper pair splitting demonstrated by two-particle conductance resonance and positive noise cross-correlation*, *Nature Communications* **3**, 1165 (2012).
 - ²⁴ M. Houzet and P. Samuelsson, *Multiple Andreev reflections in hybrid multiterminal junctions*, *Phys. Rev. B* **82**, 060517(R) (2010).
 - ²⁵ R. Mélin, D. Feinberg and B. Douçot, *Partially resumed perturbation theory for multiple Andreev reflections in a short three-terminal Josephson junction*, *Eur. Phys. J.*, **89**:67 (2016).
 - ²⁶ J.M. Byers and M.E. Flatté, *Probing spatial correlations with nanoscale two-contact tunneling*, *Phys. Rev. Lett.* **74**, 306 (1995).
 - ²⁷ J. Torrès and T. Martin, *Positive and negative Hanbury-Brown and Twiss correlations in normal metal-superconducting devices*, *Eur. Phys. J. B* **12**, 319 (1999).
 - ²⁸ M.S. Choi, C. Bruder, and D. Loss, *Spin-dependent Josephson current through double quantum dots and measurement of entangled electron states*, *Phys. Rev. B* **62**, 13569 (2000); P. Recher, E.V. Sukhorukov, and D. Loss, *Andreev tunneling, Coulomb blockade, and resonant transport of nonlocal spin-entangled electrons*, *Phys. Rev. B* **63**, 165314 (2001).
 - ²⁹ G. Deutsch and D. Feinberg, *Coupling superconducting-ferromagnetic point contacts by Andreev reflections*, *App. Phys. Lett.* **76**, 487 (2000).
 - ³⁰ G. Falci, D. Feinberg, and H. Hekking, *Correlated tunneling into a superconductor in a multiprobe hybrid structure*, *Europhys. Lett.* **54**, 255 (2001).
 - ³¹ D. Sánchez, R. López, P. Samuelsson, and M. Büttiker, *Andreev drag effect in ferromagnetic-normal-superconducting systems*, *Phys. Rev. B* **68**, 214501 (2003).
 - ³² R. Mélin and D. Feinberg, *Sign of the crossed conductances at a ferromagnet/superconductor/ferromagnet double interface*, *Phys. Rev. B* **70**, 174509 (2004).
 - ³³ J. C. Cuevas and H. Pothier, *Voltage-induced Shapiro steps in a superconducting multiterminal structure*, *Phys. Rev. B* **75**, 174513 (2007).
 - ³⁴ T. Jonckheere, J. Rech, T. Martin, B. Douçot, D. Feinberg, R. Mélin, *Multipair DC Josephson resonances in a biased all-superconducting bijunction*, *Phys. Rev. B* **87**, 214501 (2013).
 - ³⁵ J. Rech, T. Jonckheere, T. Martin, B. Douçot, D. Feinberg, and R. Mélin, *Proposal for the observation of nonlocal multipair production*, *Phys. Rev. B* **90**, 075419 (2014).
 - ³⁶ D. Feinberg, T. Jonckheere, J. Rech, T. Martin, B. Douçot, and R. Mélin, *Quartets and the current-phase structure of a double quantum dot superconducting bijunction at equilibrium*, *Eur. Phys. J. B* **88**, 99 (2015).
 - ³⁷ C. Padurariu, T. Jonckheere, J. Rech, R. Mélin, D. Feinberg, T. Martin, Yu. V. Nazarov, *Closing the proximity gap in a metallic Josephson junction between three superconductors*, *Phys. Rev. B* **92**, 205409 (2015).
 - ³⁸ R. Mélin, M. Sotito, D. Feinberg, J.-G. Caputo and B. Douçot, *Gate-tunable zero-frequency current cross correlations of the quartet state in a voltage-biased three-terminal Josephson junction*, *Phys. Rev. B* **93**, 115436 (2016)
 - ³⁹ S.N. Shevchenko, S. Ashhab and F. Nori, *Landau-Zener-Stückelberg interferometry*, *Phys. Rep.* **492**, 1 (2010).
 - ⁴⁰ J.H. Shirley, *Solution of the Schrödinger equation with a Hamiltonian periodic in time*, *Phys. Rev.* **138**, B979 (1965).
 - ⁴¹ H. Sambe, *Steady states and quasienergies of a quantum-mechanical system in an oscillating field*, *Phys. Rev. A* **7**, 2203 (1973).
 - ⁴² F. Bentosela, V. Grecchi and F. Zironi, *Oscillations of Wannier resonances*, *Phys. Rev. Lett.* **50**, 84 (1983).
 - ⁴³ B. van Heck, S. Mi, and A. R. Akhmerov, *Single fermion manipulation via superconducting phase differences in multiterminal Josephson junctions*, *Phys. Rev. B* **90**, 155450 (2014).
 - ⁴⁴ J. C. Cuevas, A. Martín-Rodero, and A. Levy Yeyati, *Hamiltonian approach to the transport properties of superconducting quantum point contacts*, *Phys. Rev. B* **54**, 7366 (1996).
 - ⁴⁵ J.C. Cuevas, A. Martín-Rodero and A. Levy Yeyati, *Shot Noise and coherent multiple charge transfer in superconducting quantum point contacts*, *Phys. Rev. Lett.* **82**, 4086 (1999).
 - ⁴⁶ D. Averin and A. Bardas, *AC Josephson effect in a single quantum channel*, *Phys. Rev. Lett.* **75**, 1831 (1995).
 - ⁴⁷ L.E. Bruhat, J.J. Viennot, M.C. Dartiaillh, M.M. Desjardins, T. Kontos and A. Cottet, *Cavity Photons as a probe for charge relaxation resistance and photon emission in a quantum dot coupled to normal and superconducting continua*, *Phys. Rev. X* **6**, 021014 (2016).
 - ⁴⁸ S. Peysson, P. Degiovanni, B. Douçot and R. Mélin, *Out of equilibrium statistical ensembles for mesoscopic rings coupled to reservoirs*, arXiv:cond-mat/0208469 (unpublished).
 - ⁴⁹ T. Nemati Aram, P. Anghel-Vasilescu, A. Asgari, M. Ernzerhoh and D. Mayou, *Modeling of molecular photocells: Application to two-level photovoltaic system with electron-hole interaction*, *J. Chem. Phys.* **145**, 124116 (2016).

⁵⁰ D.M. Basko, *Landau-Zener-Stueckelberg physics with a singular continuum of states*, arXiv:1609.01418.

The Hamiltonian

The Hamiltonian of a three-terminal Josephson junction (see Fig. 1) is the following:

$$\hat{\mathcal{H}}(t) = (12) + (13) + (14)(t) \quad (11)$$

$$(12) = \sum_{j,\mathbf{k},\sigma} \epsilon_{\mathbf{k}} c_{j,\mathbf{k},\sigma}^+ c_{j,\mathbf{k},\sigma} \quad (12)$$

$$(13) = \sum_{j,\mathbf{k}} \left[\Delta_j c_{j,\mathbf{k},\uparrow}^+ c_{j,-\mathbf{k},\downarrow}^+ + \Delta_j^* c_{j,-\mathbf{k},\downarrow} c_{j,\mathbf{k},\uparrow} \right] \quad (13)$$

$$(14)(t) = \sum_{j,\mathbf{k},\sigma} J_{j,\mathbf{k}} \left(e^{-is_j\omega_0 t} c_{j,\mathbf{k},\sigma} d_{\sigma} + e^{is_j\omega_0 t} d_{\sigma}^+ c_{j,\mathbf{k},\sigma} \right). \quad (14)$$

The first term (12) corresponds to the kinetic energy in each of the superconducting leads labels by $j \in \{S_a, S_b, S_c\}$. The second term (13) is the mean-field BCS pairing in lead j , with $\Delta_j = |\Delta_j| \exp(i\varphi_j)$. The gauge is chosen in such a way as the phase φ_j is time-independent, and the time t -dependence is in the tunnel term (14)(t). The Hamiltonian is time-periodic and, in the quartet configuration of bias voltages, we have $s_j \in \{0, \pm 1\}$. It is only in Sec. V of Supplemental Material that the wave-vector dependence of the tunnel terms is retained. The calculations presented in the remaining of the paper correspond to $J_{j,q} \equiv J_j$, and, instead of J_j , the contact transparencies are parameterized by the more usual parameters $\Gamma_j = J_j^2/W$, where W is the band-width. If Dyson equations are involved, it is then convenient to view the J_j terms as a self-energy. In this context, those J_j are denoted by Σ_j (see Supplemental Material).